

Contents lists available at [ScienceDirect](https://www.sciencedirect.com)

International Journal of Rock Mechanics and Mining Sciences

journal homepage: www.elsevier.com/locate/ijmms

The role of porosity in the dynamic disturbance resistance of water-saturated coal

Helong Gu^{a,*}, Xingping Lai^a, Ming Tao^b, Wenzhuo Cao^c, Zhengkai Yang^d

^a College of Energy Engineering, Xi'an University of Science and Technology, Xian, Shanxi, China

^b School of Resources and Safety Engineering, Central South University, Changsha, Hunan, China

^c Department of Earth Science and Engineering, Royal School of Mines, Imperial College, London, SW7 2AZ, United Kingdom

^d School of Energy and Mining Engineering, China University of Mining & Technology, Beijing, China

ARTICLE INFO

Keywords:

Water-saturated coal
Porosity
Dynamic response
Meso-deterioration

ABSTRACT

Porosity significantly affects the dynamic response of water-saturated coal and the safety of coal mine engineering in water-rich areas. For mastering the dynamic response of water-saturated coal to the porosity, this study used the coal with four levels of the porosity for dynamic tests. In this process, the dynamic compressive tests were operated on these coal specimen in both of water saturation and dry states, and the reduction factor of dynamic mechanical parameters of the coal in water-saturated state to these in dry state were focused to eliminate the effect of self dynamic properties of the coal. The results indicate that the dynamic mechanical properties non-linear positively correlate with the porosity, and its sensitivity to porosity gradually weakens as with the increase of the porosity. This effect is intuitively expressed in the dominant fracture propagation features recorded by a high-speed camera, and microscopically attributed by the size and number of microfractures around the dominant fracture. The dynamic stress intensity factor model of the dominant fracture was further established with consideration of total cohesive force for the equivalent particle on the fracture surface. It well reveals the effect mechanism of porosity on the meso-deterioration and macroscopic mechanical properties of the coal around the roadway. On this basis, the applicable conditions and suggested methods were put forward to improve the dynamic stability of water-saturated coal with various porosity.

1. Introduction

Coal mining is usually carried out in a water environment, which comes from goaf water, aquifers, water infusion, etc.^{1,2} This coal mining activities will cause the stress adjustment in surrounding coal, the mine pressure cyclical variation, and the inevitable dynamic disturbance, which will redistribute the damage in the coal, and mesoscopically manifest as the porosity variation.^{3,4} Coupled with the effect of the water, the water-solid coupling environment will be created,⁵ which significantly modified the physical properties and the mechanical response of the coal subjected to the external load.⁶ It drives many scholars to investigate the effect of the porosity on the mechanical properties of water-saturated coal, and achieved many valuable results.^{7,8} However, most of these studies focused on the effect of the porosity on static mechanical properties, and seldom involves the dynamic response of the coal to various porosity and its mechanism. Therefore, more information about the dynamic response of

water-saturated coal to the porosity should be further investigated.

Dynamic mechanical properties evaluation of the water-saturated coal various with the porosity widely involved in the coal mining activities, such as the applicable conditions selection of the coal seam water infusion, the dynamic stability evaluation of the coal in water-rich mining areas, etc.^{9,10} The fundamental access for these purpose is to obtain the effect of water infusion on the dynamic mechanical properties of coal. Subjected to the pressure water, the water-saturated coal can be assumed that the pores are filled with water, when ignore the effects of possible trapped air bubbles in the fracture. Thus it is feasible that the water content of water-saturated coal was determined by the porosity, and the role of water content on the water-saturated coal can be replaced by the porosity to some extent.⁴ Based on these, many studies were conducted to investigate the effect of porosity on the static mechanical properties of the water-saturated coal, and concluded that the strength of water-saturated coal is negatively correlated with porosity.¹¹ In fact, the water-saturated coal are usually failed in dynamic stress

* Corresponding author. College of Energy Engineering, Xi'an University of Science and Technology, Xian, Shanxi, 710054, PR China.

E-mail address: helonggu@xust.edu.cn (H. Gu).

<https://doi.org/10.1016/j.ijmms.2023.105388>

Received 13 November 2021; Received in revised form 27 November 2022; Accepted 28 March 2023

Available online 12 April 2023

1365-1609/© 2023 Published by Elsevier Ltd.

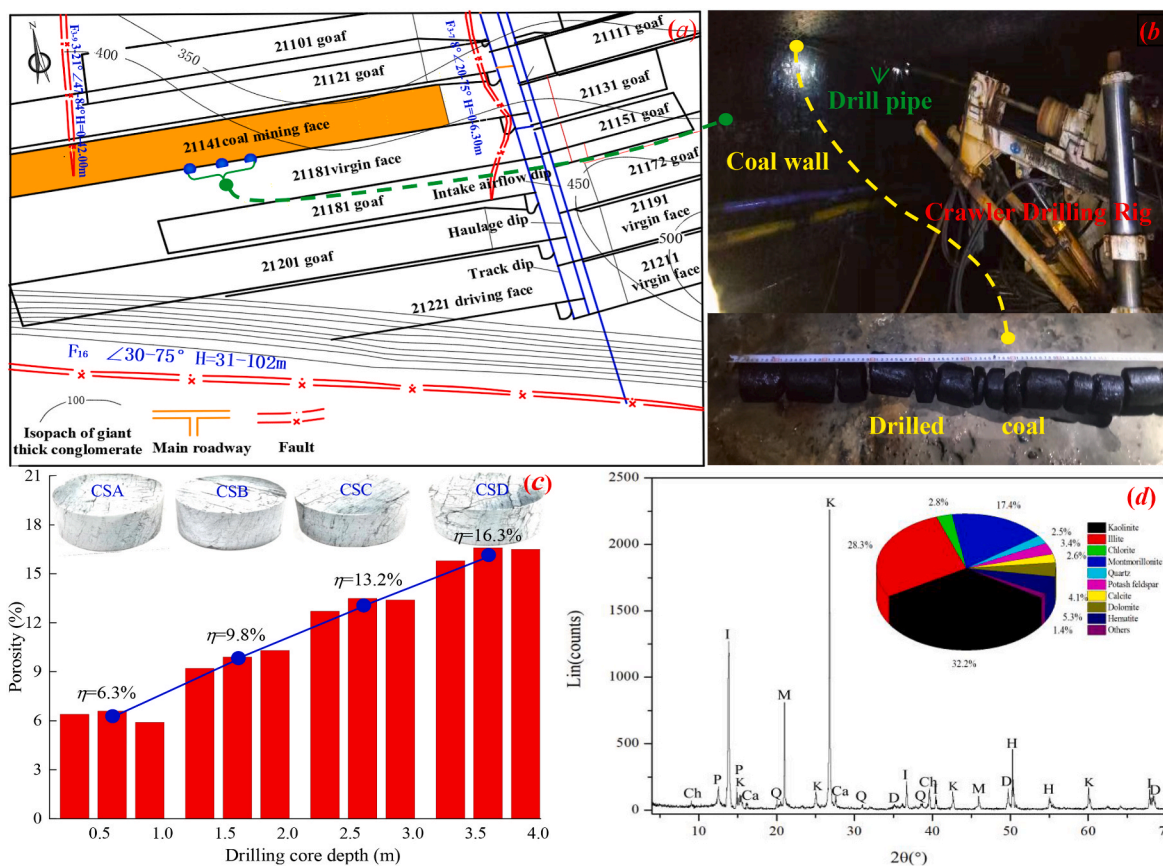


Fig. 1. Specimen information (a. drilling core site, b. drilling core equipment, c. sampling location and porosity, d. mineral composition).

environment, which usually result from the roof rupture, explosion, etc.¹² It significantly affects the mechanical response of the coal. Focusing on this problem, the previous research conducted a series of dynamic mechanical tests of coal, which involves water content, soaking time and dry-wet cycle, etc.¹³ The results indicated that the dynamic response of the coal significantly different from that of the non-coal rocks in both meso and macro aspects. However, the previous research about the role of porosity playing in the dynamic response of the coal only focused on the non-coal materials, such as water-saturated sandstone, which manifests significantly different mechanical properties from coal.¹⁴ Therefore, the effect of the porosity on water-saturated coal should be further explored.

Roadway excavation will causes the stress redistribution, and result in the local fracture accumulation, which further develop into the dominant fracture. It verify the sensitivity of the fracture in the coal during the fracture evolution process subjected to the dynamic disturbance, and dominant the dynamic mechanical properties of coal. Coal is a kind of fracture body, which contains different scales of fractures, varies from micro to macro. The dominant fractures propagation process manifest as both of its length and connected micro fractures increases. In both the formation and expansion process of the dominant fracture, a large number of microfractures are connected around the dominant fracture under the effect of the complex static stress. It macroscopically manifest as the bifurcation phenomenon of fractures. The bifurcation here refers to the extended state, not the extended path of the dominant fracture.

Coal dynamic failure is usually characterized by the fracture initiation, propagation, and coalescence with associated damage and evolution, which determined by both the fracture toughness and dynamic stress intensity factor (SIF).¹⁵ Assuming the microfractures around the dominant fracture are not connected with each other, the randomly distributed micro fracture will divided the fracture surface into various

scales of the dependent equivalent particles. In this case, the dynamic stress between the dominant fracture surface, which determines the dynamic SIF, can be converted into the total dynamic cohesive force among particles. Meanwhile, the average size and particle number on the fracture surface determine the length of the dominant fracture. Thus the fundamental cause of fracture propagation can be simplified as the variation of the micro-mechanics between the total particles on dominant fracture surface under dynamic loads, and the variation of the porosity can be reflected in the size and number of the equivalent particles that composed the fracture surface. It excellently overcomes the difficulty that the previous single fracture analysis can't reveal the effect mechanism of porosity due to its randomness distribution and non-uniformity in equivalent particle size. It provides the possibility to reveal the dynamic response mechanism of the water-saturated coal to porosity. The main forces among the particles include van der Waals, electrostatic, and liquid bridge forces. The liquid bridge force consists of two parts: static and dynamic.¹⁶ There are several methods to calculate the cohesive force, which usually be classified as the Laplace-Young's exact numerical solution method and the Fisher's approximate solution theory method.¹⁷⁻¹⁹ Both of the methods can only calculate the cohesive forces between two particles, but not adequate for modelling the effect of the particle number in the fracture surface for the water-saturated coal with different porosity. Thus, more information about the total dynamic cohesive force among particles on both sides of the dominant fracture surface should be obtained.

Based on the above analysis, this study attempts to obtain the effect and its mechanism of the porosity on the dynamic mechanical properties of the water-saturated coal. To avoid the effects of the physical and mechanical properties of the coal itself, the reduction factor of the dynamic mechanical parameters of water-saturated coal to those of dry coal were set as the object to compare the dynamic response of water-saturated coal with various porosity. On this basis, the porosity effect

Table 1
Physical and dynamic mechanical parameters of coal.

Group name	Dynamic strength (MPa)		Dynamic elastic modulus (GPa)		Strain rate (s ⁻¹)		Density (g.cm ⁻³)		Porosity (%)
	Dry	Water saturation	Dry	Water saturation	Dry	Water saturation	Dry	Water saturation	
CSA	37.2	32.5	7.86	7.09	97.5	98.9	1.545	1.605	6.4
	34.1	31.3	7.14	7.05	98.6	96.7	1.523	1.586	6.6
	37.4	33.4	7.36	6.50	102.5	99.5	1.561	1.610	5.9
CSB	34	27.6	6.86	6.36	98.8	97.8	1.502	1.593	9.2
	33.1	27.1	6.50	5.82	100.3	99.6	1.486	1.582	9.9
	30.4	27.3	6.95	6.00	98.8	100.8	1.467	1.568	10.3
CSC	31.5	23.3	6.36	5.59	98.2	95.8	1.374	1.498	12.7
	29.1	23.2	6.27	5.23	102.3	98.7	1.321	1.455	13.5
	28.5	21.8	6.77	5.32	95.9	97.8	1.318	1.451	13.4
CSD	26.3	19.7	6.00	4.82	98.0	100.8	1.293	1.450	15.8
	24.3	17.5	6.23	4.73	97.2	96.8	1.275	1.439	16.6
	26.2	18.2	5.86	5.00	99.8	98.9	1.262	1.426	16.5

model for the fracture expansion of water-saturated coal was established with the consideration of the total cohesive force among the equivalent particles on the dominant fracture. These studies are critical for the reinforcement of coal seam roadways.

2. Specimen preparation and basic properties test

Coal seam roadway excavation will adjust the stress distribution in the surrounding coal subjected to the effect of in-situ stress, which will cause the damage of the surrounding coal manifest as a non-linear variation as with the enhancement of the depth relative to the roadway surface.^{20,21} It microscopically expressed as the porosity variation to some extent. To study the effect of porosity on water-saturated coal, the surrounding coal of the air-return roadway in the 21,141 coal mine face of Qianqiu coal mine was selected as the sample drilling site, as shown in Fig. 1(a). The coal type used in this study is long-flame coal. It is black block, with asphalt luster, dry, loose and broken, and easy to self ignite. The loosening depth at sampling position is 3.5 m, and the coal seam thickness is 10 m. To obtain coal samples with different

porosity, a core drill bit with an outer diameter of 122 mm and an inner diameter of 85 mm was applied to drill a hole with a depth of 4 m in the roadway surrounding coal to obtain the drill core, as shown in Fig. 1(b). Based on the lab integrity test of the coal samples at different depths, the sample were divided into four different groups, that is, CSA, CSB, CSC, and CSD, respectively. The integrity among the groups is significant different, but approximately the same in each group.

According to the specifications of the International Society for Rock Mechanics (ISRM),²² all samples were manufactured into cylindrical specimen with both a diameter and axial length of 50 mm. The end surfaces were polished with a roughness below 0.02 mm and perpendicular to the axis within 0.001 radian. Based on the existing grouping, each group such as group CSA, was randomly divided into two groups, CSA1 and CSA2, to prepare the dry and water-saturated coal specimens, respectively. To make the coal fully water saturation and detach the air in the pores, a forced suction apparatus was applied to prepare the water-saturated coal specimens. The simultaneous forced suction of six specimens can be realized at an infusion pressure of 2 MPa, which was detailed in our previous study.⁶ To reduce the effect of water infusion on

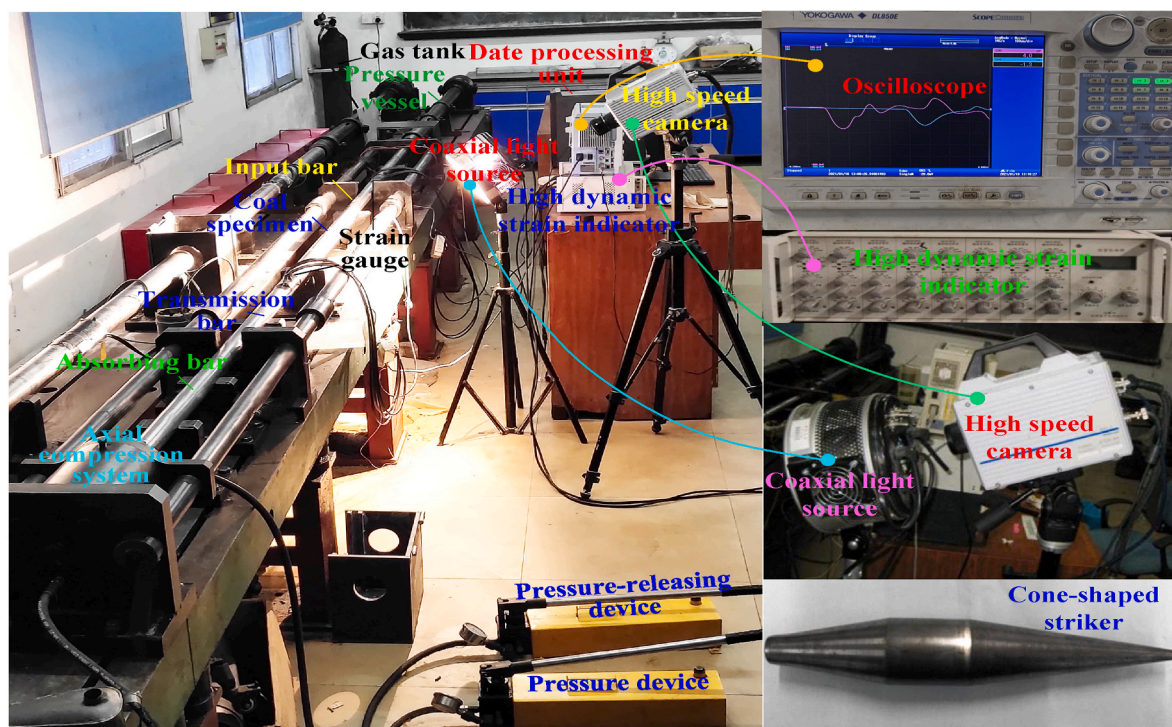


Fig. 2. Configuration of the SHPB system in laboratory.

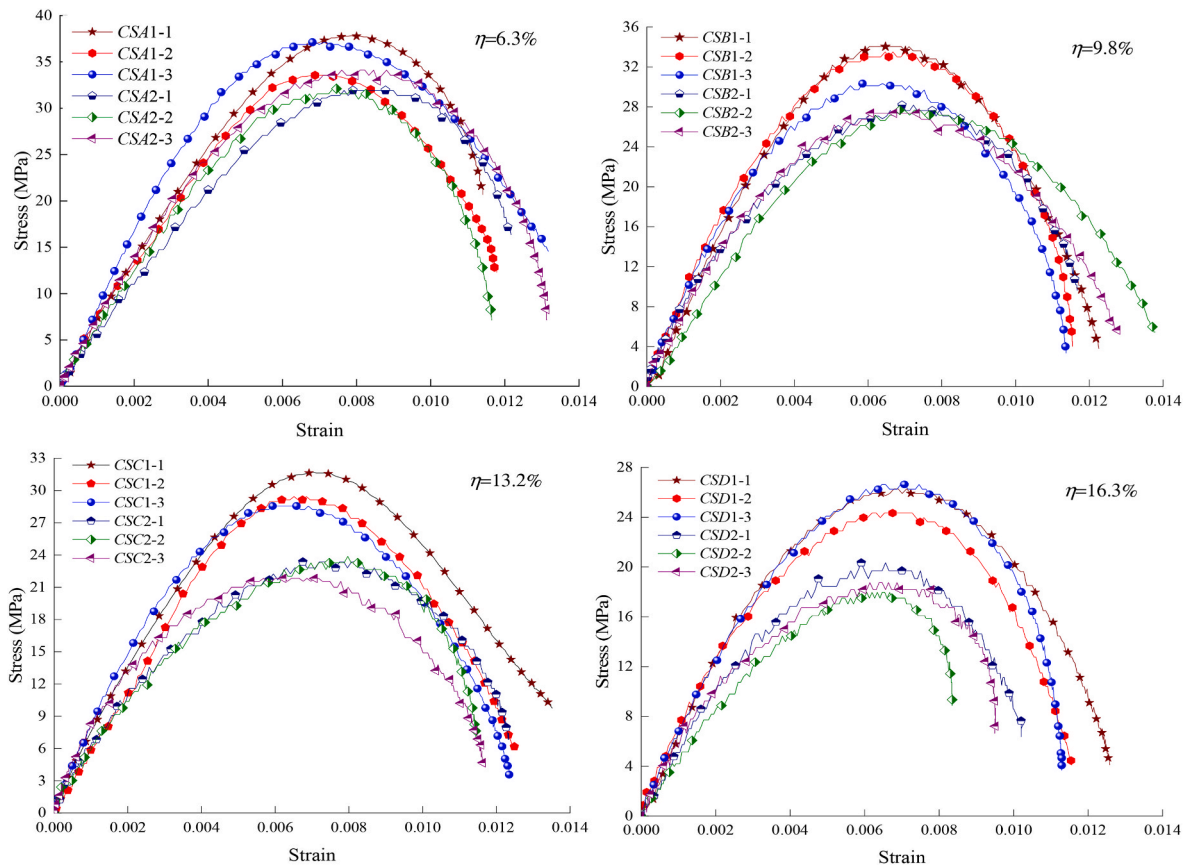


Fig. 3. Dynamic stress-strain curves of water-saturated coal with different porosity.

the internal fracture of the coal, the dry specimens were forced to absorb water inside the apparatus with an infusion pressure of 0.5 MPa until the volume of the infiltration water equaled the volume of the seepage water. Thereafter, they were removed from the apparatus and weighed.

The porosity of the coal was measured through the following two methods: namely cryogenic liquid nitrogen method and 300-point counting of thin-section method. The average porosity obtained by the two methods were used in this study. To obtain the density of coal before and after water saturation, the bulk volume of the specimen was calculated according to the diameter and height, and measured using a Vernier calliper with an accuracy of 0.02 mm, where the density is the mass to volume ratio. The parameters obtained from these tests are shown in Table 1. It can be concluded that the integrity of the coal relative correlate with the porosity, and the average porosity η of the CSA, CSB, CSC, and CSD group were 6.3%, 9.8%, 13.2% and 16.3%, respectively, and the typical specimen is shown in Fig. 1(c). In addition,

the mineral composition was determined by X-ray diffraction (XRD), and the test results are shown in Fig. 1(d). It can be seen that coal is composed of a variety of minerals, including soluble minerals such as dolomite, chlorite, etc. and insoluble minerals such as kaolinite and quartz. Due to the short water infusion time and the low content of soluble minerals in the coal, the water-coal chemical interaction was ignored in the research process. In this case, the mineral composition of the coal specimen remain unchanged before and after the water saturation process.

3. Dynamic compression test and analysis

To test the dynamic response of the water-saturated coal to porosity, the water-saturated and dry coal with different porosity were tested with the modified Split Hopkinson Pressure Bar (SHPB), which can realize the coupled static and dynamic loads of the coal specimen.²³ The

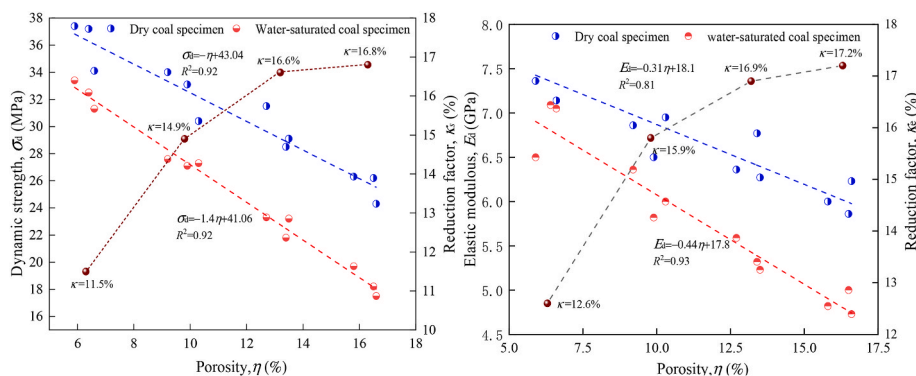


Fig. 4. Dynamic mechanical parameters of water-saturated coal various with the porosity (a. dynamic strength, b. dynamic elastic modulus).

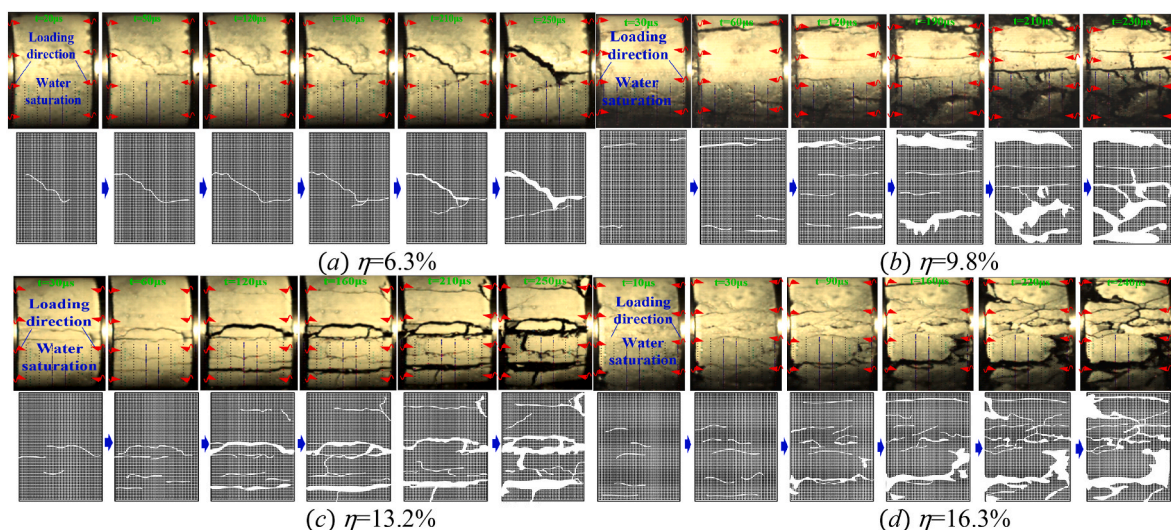


Fig. 5. Fracture dynamic evolution process for the coal specimen with different porosity.

configuration of the modified SHPB system was shown in Fig. 2 and described in detail in previous studies.²⁴ To avoid discreteness of the dynamic properties, three specimens were tested under approximately the same strain rate ranging from 94 s^{-1} to 105 s^{-1} . The typical stress-strain curves for each group of the coal specimens under dry and water-saturated states were shown in Fig. 3. It demonstrate that the porosity and water saturation significantly affect the dynamic stress-strain curves of the coal, which mainly manifest in the dynamic

strength and elastic modulus. It can be concluded that the water saturation can significantly affect the dynamic strength and elastic modulus of the coal, and the effect degree determined by the porosity.

The multiple factors, such as the pore structure and fracture distribution, inevitably affect the dynamic mechanics of the coal. To avoid these disturbances, the reduction factors of the dynamic mechanical parameters of water-saturated coal to those of dry coal were set as the index to compare the effect of porosity on water-saturated coal. To

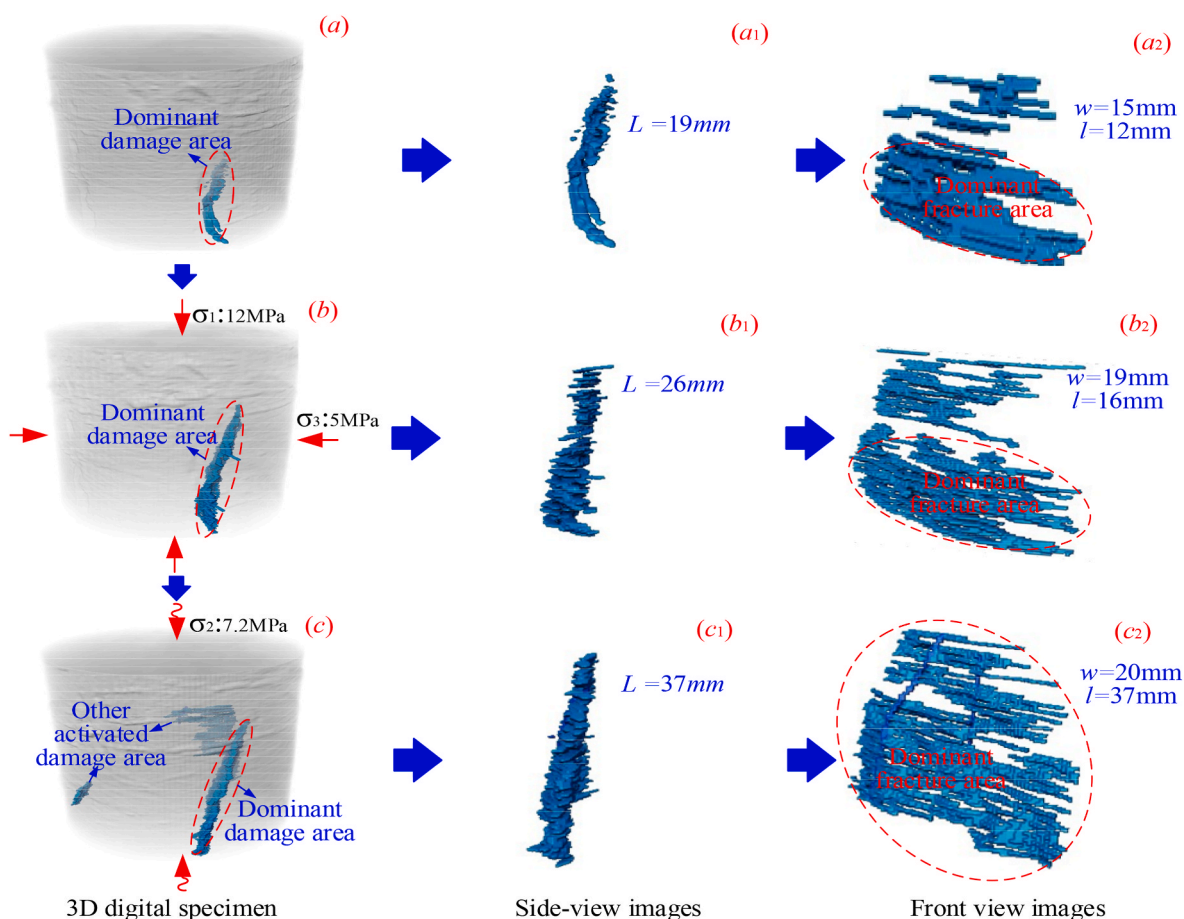


Fig. 6. Evolution characteristics of dominant fractures in coal specimen subjected to dynamic load.

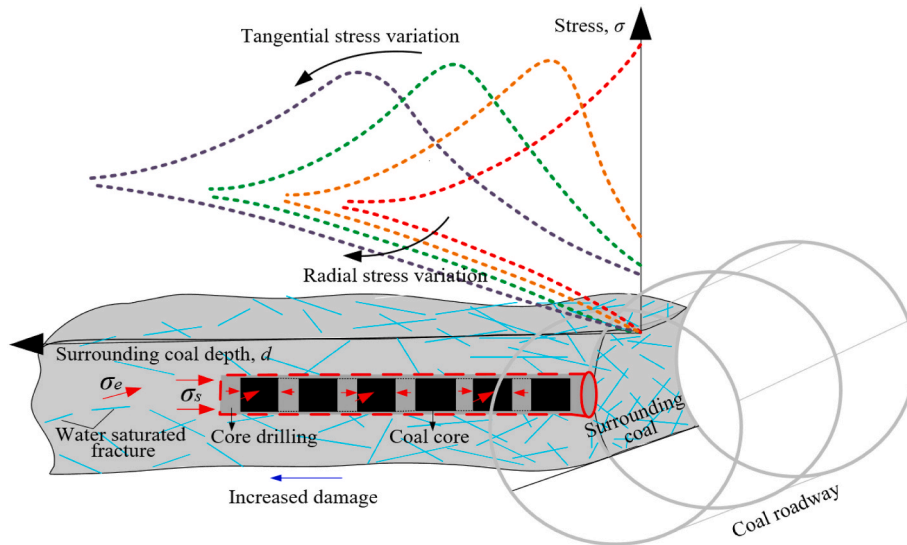


Fig. 7. Schematic diagram about the effect of porosity on the microstructure of the coal.

detailed describe the effect of the porosity on the water-saturated coal, k_s and k_e were set as the reduction factors of the dynamic strength and elastic modulus of the water-saturated specimen to those of the dry specimen, respectively, which can be expressed as follows:

$$k_s = \frac{\sigma_{ad} - \sigma_{as}}{\sigma_{ad}} \quad (1)$$

$$k_e = \frac{E_{ad} - E_{as}}{E_{ad}} \quad (2)$$

where σ_{ad} and σ_{as} are the average dynamic strength of the dry and water-saturated specimen, respectively, and E_{ad} and E_{as} represent the average elastic modulus of the dry and water-saturated specimens, respectively.

The detailed differences in the dynamic strength and elastic modulus between dry and water-saturated coal are shown in Fig. 4, where the dynamic strength is the stress peak of the stress-strain curve and the dynamic elastic modulus is usually ratio of the 50% of the coal's

dynamic strength value to its corresponding longitudinal strain value.²⁵ It can be concluded that the sensitivity of the dynamic mechanical properties of coal to water amount is positively correlated with the porosity. Specially, with an increase of porosity, the reduction factors of the dynamic strength and elastic modulus increase with a gradually decreasing amplitude. The detailed test results are shown in Table 1.

Coal is an aggregate of fracture. Its destruction process manifest as the fracture dynamic evolution. To record the fracture dynamic propagation process subjected to the dynamic load, a high-speed camera (FASTCAMSA1.1) was applied to record the fracture evolution process, whose frame rate was set to 100,000 fps. In this case, the camera records the fractures distribution on the surface of the specimen every 10 μ s. The detailed information on this apparatus was described in our previous study.²⁶ To better illustrate the effect of water saturation on the fracture propagation, the typical failure processes of the dry and water-saturated coal specimens in each group were compared, as shown in Fig. 5. It exhibits the typical fracture evolution process of the coal with different

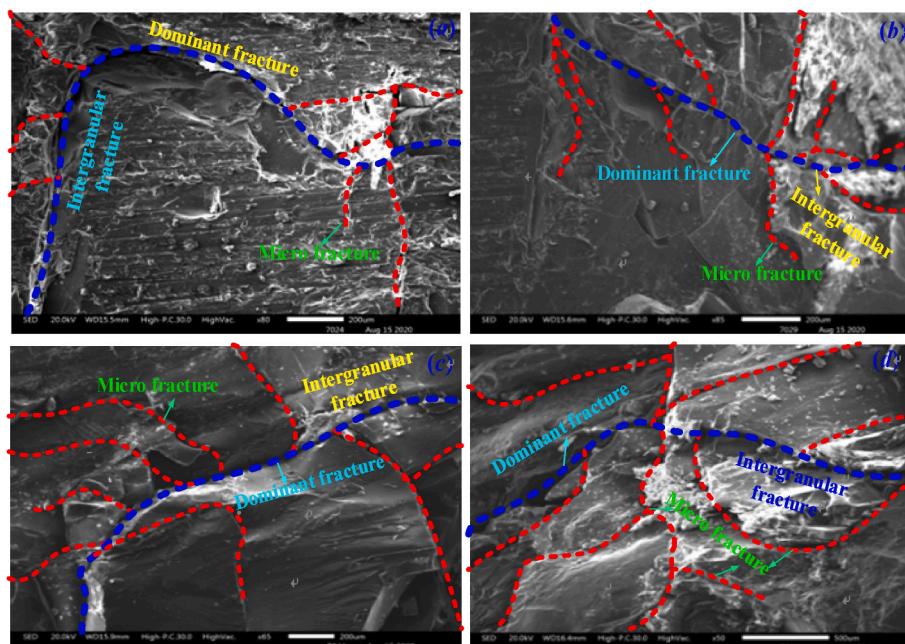


Fig. 8. Microstructure of coal specimen with different porosity (a. $\eta = 6.3\%$, $\eta = 9.8\%$, c. $\eta = 13.2\%$, d. $\eta = 16.3\%$).

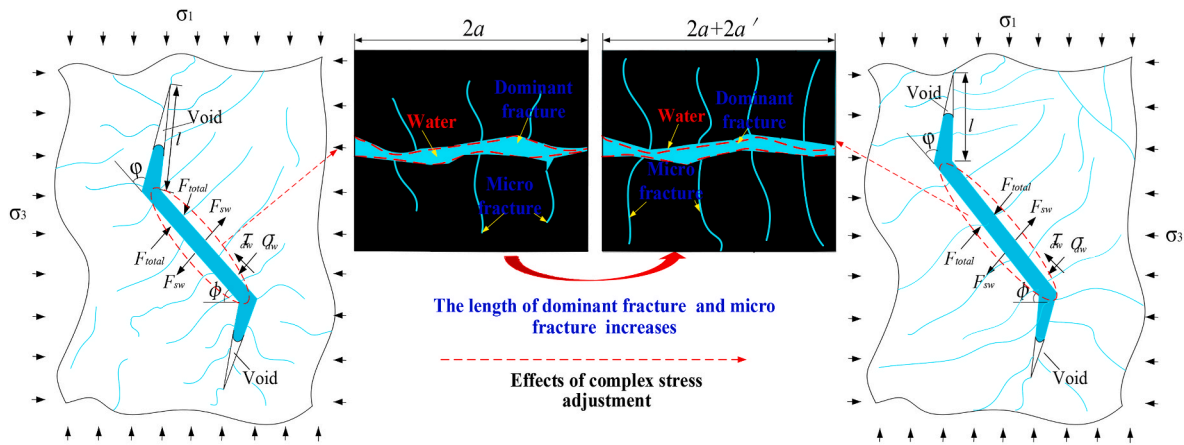


Fig. 9. Schematic diagram about the effect of porosity on the microstructure of the coal.

porosity. It can be concluded that coal dynamic failure process controlled by several dominant fracture propagation. Its propagation direction are substantially parallel to the dynamic loading direction. Thereafter, these fractures mainly manifest as the increase of the width and the length of the dominant fracture, which belongs to a typical splitting failure.

4. Dynamic failure mechanism of water-saturated coal

4.1. Microscopic properties

The fracture evolution process is the macroscopic manifestation of the microstructure dynamic development. In this process, the microscopic fracture structure, fracture propagation characteristics, the cementation type between particles, etc. significantly affect its macro-mechanical properties of the coal.²⁷ To investigate fracture distribution characteristics in the coal specimens around the roadway and its response under static and dynamic stress, the 3D digital specimen was obtained with the aid of the CT 3D reconstruction technology. For better comparing the information about the effect of static and dynamic load variation on the fracture evolution, the dominant damage area were extracted as object and it was further divided into the side view and front view, as shown in Fig. 6. Here, L is the length of dominant damage area along the principal stress direction, w and l are the width and the length of dominant fracture area, respectively. It can be concluded that the dominant damage is composed of many complex fracture networks. The mutual concatenation and expansion of these fractures create the dominant fracture area.

With the static stress variation around the specimen, the length and width of the dominant damage area enhancement, but no significant variation in microfractures density, as shown in Fig. 6(a). Before sample drilling, roadway surrounding coal stress adjustment process modified the loading conditions around the specimen. The loading stress variation around the sample results in the formation, expansion and concatenation of micro fractures, and expedites the generation of dominant fracture, as shown in Fig. 7. This phenomenon consistent with the previous research results, that is, the coal failure under static load mainly manifest as the dominant fracture propagation, and other micro fractures are restrained in this process.²⁸

When subjected to the dynamic load, the dominant fractures manifest the similar propagation behavior as with that under the surrounding static stress. What the difference is that the dominant fracture area are mainly characterized by the length increase, but the width of the dominant fracture area was not significantly changed. In addition, When subjected to dynamic load, different scales of the damage area in coal are almost simultaneously activated and expanded,²⁹ which is another significant difference compared with that under static stress. The dominant

fracture extension connect the existing microfractures, which will further enhance the microfracture number around the dominant fractures, as shown in Fig. 8. Therefore, the static stress redistribution caused by roadway excavation can activate the local damage and make it develop into the dominant damage area. It results in the fractures propagation sensitivity difference during the dynamic loading process, and drives the dominant fracture area expansion.³⁰

To further explore the fracture distribution in dominant fracture area, the micro structure of the coal was investigated with the aid of scanning electron microscope. Subjected to the dynamic disturbance, a large number of internal fractures in the water-saturated specimen were activated to form a complex fracture network, which characterized by different scales of the secondary fractures around the dominant fracture, as shown in Fig. 9. The effect of pressurized water makes the weak connection between the fracture surfaces destroy to a certain extent, which cause the interconnection among fracture surfaces approximately present as the pore cementation. In this case, the two sides of the dominant fracture can be regarded as different sizes of the dependent particles. Subjected to the effect of the porosity, the size and number of the particles show the significant differences, which will redistribution the stress on the dominant fracture surface, and further affect the fracture expansion.

4.2. Effect mechanism of the porosity on the water-saturated coal

The variation in strength concurrent with dominant fracture propagation is an essential element in describing the deformation.³¹ The length and width expansion of the dominant fracture are the fundamental reason for the coal failure subjected to dynamic load. Based on the obtained porosity and quality difference between dry coal and water-saturated coal, the pores inside the coal specimen can be considered to be fully filled with the water. When subjected to the dynamic load, a single pore and the zone of reduced stress surrounding that pore cannot propagate rapidly enough to prevent other smaller or poorly-oriented pores from later being activated. It will inhibit the pore water pressure gradient generation.

Dominant fractures expansion determine the dynamic failure of coal. It is determined by the coupled effect of the fracture dynamic stress intensity factor (SIF) and dynamic fracture toughness. It closely correlate with the stress distribution on the dominant fracture surface.³² In recent years, researchers have studied the mechanical properties of coal under dynamic loads by analyzing the initiation and propagation of fractures and proposed several micromechanic models. Among them, the sliding fracture model is widely accepted.³³ In this study, a three dimensional water-bearing wing fracture was simplified as a plane fracture. The fracture was then analyzed as a single fracture to determine the influence of the external load. Given this situation, the

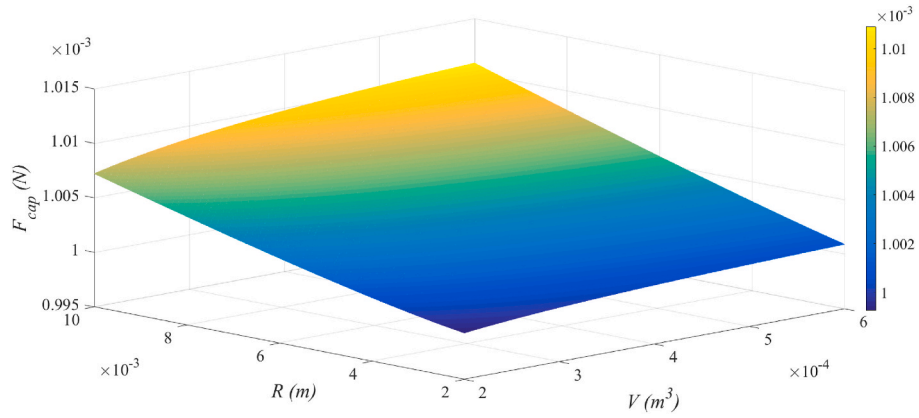


Fig. 10. The variation of the average cohesive force with the average radius R and liquid bridge volume V .

complete closed wing fracture was analyzed as the research objective. Therefore, to analyze the failure mechanism of the specimen under external load, the single wing fracture as the research object to explore the fracture expansion, as shown in Fig. 9. The coal is an aggregate of fractures with different sizes of fractures inside, various from micro to macro. The microfracture interconnected with each other, and the distributed micro fracture will divided the dominant fracture surface into different scales of parts, which can be regarded as dependent unequal-size particles on the dominant fracture surface.

During the dynamic loading process, the dominant fractures are activated and expand preferentially. Subjected to the Stephen effect, the rapid expansion of water-containing fractures produces dynamic cohesive force between the fracture surface.³⁴ In this case, the dynamic stress between the fracture surface can be converted into the total dynamic cohesive force among dependent particles on fracture surface. Thus the fundamental cause of fracture propagation can be simplified as the variation of the micro-mechanics between the total particles on the dominant fracture surface under dynamic loads, and the variation of the porosity can be reflected in the size and number of particles that composed the dominant fracture surface.

To characterize this effect, the total dynamic cohesive force is proposed, which represents the dynamic cohesive force that the dominant fractures expansion needs to overcome. It gets rid of the limitations that the dynamic cohesive force between two particles cannot characterize the dynamic cohesive force between the fracture surfaces. Formally, it can be expressed as the sequential integration of the average dynamic cohesive force among particles on the number of liquid bridges that needs to overcome during the fracture expansion. The length of microfractures around the dominant fracture can be equivalent to the comprehensive effect of particle size and the liquid bridge volume between the particles. To calculate the cohesive force between particles, many previous studies have been conducted and achieved many valu-

able results. The cohesive force between particles is mainly manifested as the liquid bridge force between the particles, which can be divided into dynamic liquid bridge force, static liquid bridge force and the attraction force between particles. In the calculation process, because the latter is much smaller than the dynamic and static liquid bridge forces, the attraction force between particles is usually ignored. The dynamic cohesive force F_{cap} between the equal particles can be expressed as follows³⁵:

$$F_{cap} = F_{vis} + F_{sta} \quad (3)$$

where F_{sta} , F_{vis} are the static liquid bridge force and dynamic liquid bridge force, respectively which is expressed in Eqs (4) and (5).

$$F_{sta} = 2\pi R\sigma \cos \theta \left[1 - \frac{1}{\sqrt{1 + \frac{2V}{\pi R D^2}}} \right] \quad (4)$$

$$F_{vis} = \frac{3\pi\delta R^2}{2D} v \quad (5)$$

where D is the surface distance between two unequal spheres with the average radius R ; θ is the solid/liquid contact angle; δ is the fluid viscosity; V is the liquid bridge volume; σ is the interfacial tension between the water and particles surface; v is relative movement velocity between two particles.

Thus, the average cohesive force between particles can be expressed as:

$$F_{cap} = 2\pi R\sigma \cos \theta \left[1 - \frac{1}{\sqrt{1 + \frac{2V}{\pi R D^2}}} \right] + \frac{3\pi\delta R^2}{2D} v \quad (6)$$

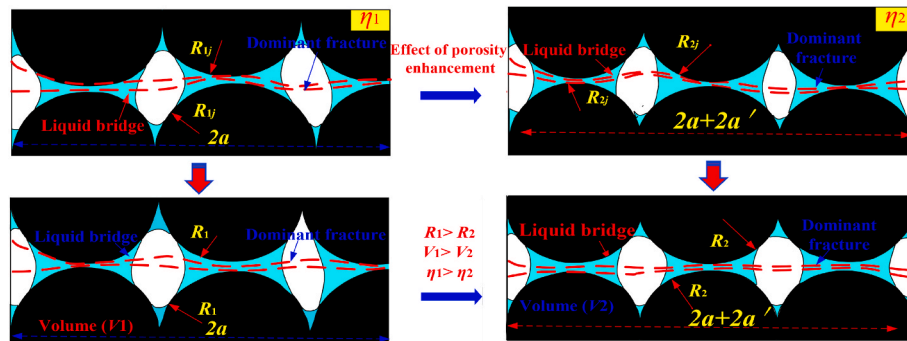


Fig. 11. Simplified model about the effect of porosity on the particle distribution in the fracture surface.

To detailed explain the variation of the average cohesive force with the porosity, the parameters in the equation were determined based on the reference³⁶: $D = 0.03$; $\delta = 0.89 \times 10^{-3}$ Pa s; $\sigma = 72$ mN/m; $\theta = 30^\circ$; $\alpha = 0.3$. In addition, according to the fracture expansion speed, the relative moving speed of the particles was estimated as $v = 1.6$ m/s. In this case, Eq (6) becomes a average cohesive force with two degree of freedom, that is, the variables are average radius R and liquid bridge volume V . The variation of the average cohesive force with the two degree of freedom is shown in Fig. 10.

It can be concluded that the average cohesive force non-linear positively correlate with both the particle radius and the liquid bridge volume. It illustrates that the reduction of the particle size and the liquid bridge volume induced by the enhancement of the porosity will weaken the dynamic cohesive force among particles. However, this equation cannot characterize the increase of the number of the liquid bridges caused by the increase of the porosity, which significantly affect the dominant fracture propagation.

To study the effect of different porosity on the liquid bridges number among the dominant fracture surface in the fracture expansion process, the two particle groups with the different length along the fracture propagation direction was applied as the analysis object, as shown in Fig. 11. To better illustrate the effect of particle number, it is assumed here that the particles on the dominant fracture surface are closely connected, and the distances between the corresponding particles in the two fracture surfaces are equal for the coal with different porosity. The corresponding particles on both sides of the fracture surface following the relationship:

$$\frac{1}{R_1} = \frac{1}{R_{1i}} + \frac{1}{R_{1j}} \quad (7)$$

$$\frac{1}{R_2} = \frac{1}{R_{2i}} + \frac{1}{R_{2j}} \quad (8)$$

where R_1, R_2 represent the average particle radius on both fracture surfaces when the porosity of the coal are η_1, η_2 , respectively; $R_{1i}, R_{1j}, R_{2i}, R_{2j}$ represent the radius of each corresponding particles on both sides of the fracture, which arranged at intervals in the fracture surface for the coal with the porosity of η_1 and η_2 .

Due to the close relationship between the particles in the dominant fracture surface, the number of liquid bridges n that need to be overcome during the fracture expansion, respectively.

$$n \approx L/R \quad (9)$$

where R is the average particle radius, L represent half of the main fracture length for the dominant fracture. For the coal with the porosity of η_1 and η_2 , L can be expressed as a and $(a+a')$, respectively.

Therefore, the required total cohesive force F_{total} can be expressed as the number of liquid bridges that need to be overcome in dominant fracture propagation process multiplied by the average cohesive force, which can be expressed as:

$$F_{total} = nF_{cap} \quad (10)$$

$$F_{total} = 2\pi L \sigma \cos \theta \left[1 - \frac{1}{\sqrt{1 + \frac{2V}{\pi R D^2}}} \right] + \frac{3\pi \delta R L}{2D} v \quad (11)$$

For a single particle cluster, the average volume of the liquid bridge can be expressed as³⁷:

$$V = \frac{16\pi \eta R^4}{3(1-\eta)} \quad (12)$$

Integrating Eqs (11) and (12), it can be concluded that:

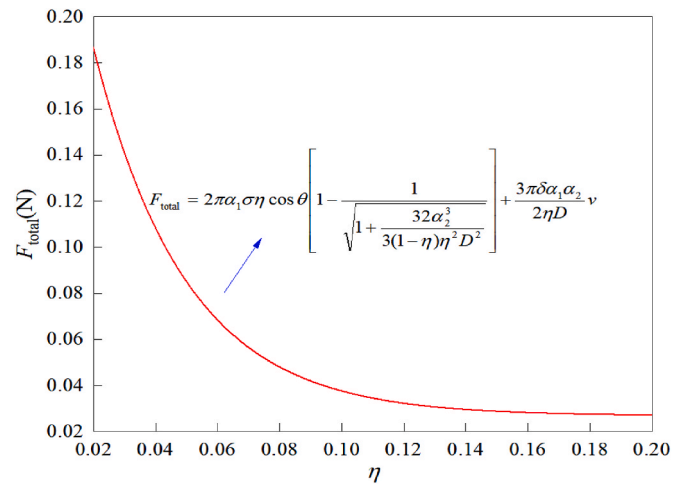


Fig. 12. The F_{total} for the dominant fracture of the water-saturated coal various with the porosity.

$$F_{total} = 2\pi L \sigma \cos \theta \left[1 - \frac{1}{\sqrt{1 + \frac{32\eta R^3}{3(1-\eta)D^2}}} \right] + \frac{3\pi \delta R L}{2D} v \quad (13)$$

The above analysis manifest that the length and the width of the dominant fracture area are positively related to the porosity, which indicates that both the length of the dominant fracture and the micro fractures around it increases. The enhancement of the latter will modify the shape parameter, and reduce the equivalent radius of particles, that is, the equivalent radius R negatively correlated with the porosity. Here L and R are set to be:

$$L = \alpha_1 \eta R = \frac{\alpha_2}{\eta} \quad (14)$$

where α_1 and α_2 are constants. Considering that the microfracture length variation has little effect on the R for the equivalent particles around the dominant fracture, here $\alpha_1 \gg \alpha_2$.

$$F_{total} = 2\pi \alpha_1 \sigma \eta \cos \theta \left[1 - \frac{1}{\sqrt{1 + \frac{32\alpha_2^3}{3(1-\eta)\eta^2 D^2}}} \right] + \frac{3\pi \delta \alpha_1 \alpha_2}{2\eta D} v \quad (15)$$

To detailed explain the variation of the total cohesive force with the porosity, the parameters in the equation were determined as the above settings, and the R, α_1 and α_2 were set as 0.002 m, 3 and 0.1, respectively. In this case, Eq (15) becomes a total cohesive force with one freedom of the porosity, that is, the variable is only the porosity. The variation of the total cohesive force with the increase of the porosity is shown in Fig. 12.

It can be concluded that the total cohesive force is negatively correlate with the porosity. The sensitivity of the total cohesive force to porosity gradually decreases, and the specifically manifest as that with the porosity increases, the reduction amplitude of the total cohesive force gradually decreases. Thus, it can be obtained:

$$F_{total-\eta_1} < F_{total-\eta_2} \quad (16)$$

It indicates that under dynamic loading, with the increase of porosity, the total dynamic adhesive force F_{total} on the dominant fracture surface will increase. The force to restrain the fracture expansion will be enhanced to a certain extent, which will verify the stress distribution on the dominant fracture surface.

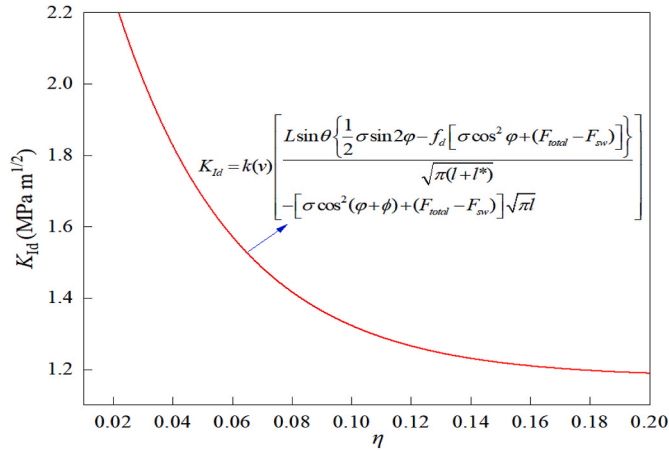


Fig. 13. The dynamic SIF K_{Id} of water-saturated coal various with the porosity.

The dynamic SIF is not only correlate with the F_{total} , but also closely related to other factors. Under dynamic load, the fracture propagation lag behinds the dynamic load rate, which accompanied the stress distribution variation. In this condition, the normal stress σ_{ds} and effective shear stress τ_{ds} on the dominant fracture surface can be expressed as follow²⁷:

$$\tau_{ds} = 0.5\sigma \sin 2\varphi - f_d \sigma \cos^2 \varphi \quad (17)$$

$$\sigma_{ds} = \sigma \cos^2(\varphi + \varphi) \quad (18)$$

With the consideration of the Stephen effect in the dominant fracture propagation process, the total cohesive stress F_{total} will prevent the fractures from propagation. Taking into account the smaller free water squeezing force F_{sw} on the fracture surface compared with the total cohesive stress F_{total} , the stress distribution on the main fracture surface can be express as:

$$\tau_{dw} = \frac{1}{2}\sigma \sin 2\varphi - f_d [\sigma \cos^2 \varphi + (F_{total} - F_{sw})] \quad (19)$$

$$\sigma_{dw} = \sigma \cos^2(\varphi + \varphi) + (F_{total} - F_{sw}) \quad (20)$$

where f_d is the dynamic friction coefficient of the fracture.

It can be concluded from Eqs. (19) and (20) that the participation of water will reduces the normal stresses, but enhances the effective shear stress on the fracture surface.

For the coal, the dynamic SIF is a key parameter to describe the difficulty of fracture expansion.³⁸ The above macro and meso failure characteristics of the coal indicated that the fracture type of rock material is class I. When subjected to resistance stress F_{sw} and total cohesive force F_{total} caused by free water in the fracture, the wing fracture model was modified, and the dynamic SIFs of the fractures can be expressed as:

$$K_{Id} = k(v)K_I = k(v) \left[\frac{2\alpha\tau_{dw} \sin \theta}{\sqrt{\pi(l+l^*)}} - \sigma_{dw} \sqrt{\pi l} \right] \quad (21)$$

where $k(v)$ is the coefficient of the fracture propagation rate,³⁹ l^* is equivalent wing fracture length.

Integrating Eqs (19)–(21) can obtain:

$$K_{Id} = k(v)K_I = k(v) \left[\frac{L \sin \theta \left\{ \frac{1}{2} \sigma \sin 2\varphi - f_d [\sigma \cos^2 \varphi + (F_{total} - F_{sw})] \right\}}{\sqrt{\pi(l+l^*)}} - [\sigma \cos^2(\varphi + \varphi) + (F_{total} - F_{sw})] \sqrt{\pi l} \right] \quad (22)$$

To detailed explain the variation of the dynamic SIF various with the

porosity, the parameters in Eq (22) were determined as the above settings, and the $k(v)$, l^* , θ , φ , φ , and f_d were set as 1.3, 0.003 m, 15°, 30°, 30° and 0.22, respectively. The variation of the dynamic SIF K_{Id} with the increase of the porosity is shown in Fig. 13. It can be concluded that the dynamic SIF of water-saturated coal gradually decreases with a gradual decrease amplitude as the enhancement of the porosity, which indicate that its sensitivity to the porosity gradually decline.

The fracture expansion is coupled determined by the effect of the fracture dynamic SIF and dynamic fracture toughness. For type I fracture, the fracture mainly manifest as the intergranular propagation and determined by the dynamic cohesive force between the particles around the tip of the fracture. For dynamic SIF, the dynamic load activates the overall particles in the fracture surface, which involves all particles in one fracture surface to the other corresponding fracture surface. Different from that, the fracture dynamic expansion in the fracture tip manifest as the overcome of the cohesive force between particles one by one. In this process, except for the fracture toughness of coal in dry state, the dynamic fracture toughness mainly involves the dynamic cohesive forces between on set of the corresponding particles. Due to the dynamic cohesive force between individual particles is very small,¹² this increment variation has little effect on the fracture expansion, and the dynamic SIF variation should be mainly focused on.

The above research illustrate that the effect of porosity on the fracture can reducing the dynamic fracture toughness and dynamic SIF of coal. It illustrates that the enhancement of porosity will promote the fracture expansion, which macroscopically manifest as the enhancement of fracture number subjected to dynamic load, as shown in Fig. 5. This promotion effect is significant for coal seams with small porosity. As the porosity increases, the sensitivity of the dynamic SIF to the porosity gradually weaken, which macroscopically manifest that as the reduction latitudes of the dynamic mechanical parameters of water-saturated coal relative to these of the dry coal were gradually reduced, as shown in Figs. 3 and 4.

5. Discussion on efficient methods for dynamic disaster instability

Coal seam water infusion is widely used in the coal burst prevention due to its diverse disaster prevention capabilities and complex prevention mechanisms. Its function result from the pressure water seepage in the coal seam, which accompany the modification of the coal seam.³⁸ This modification in the laboratory represent as the variation of the dynamic mechanical properties of the water-infused coal. Its effect exertion depends on the dynamic softening effect of water infusion on the coal, which is closely related to the porosity. The experimental results show that as the porosity increases, the dynamic mechanical properties of the coal present as a non-linear decreasing trend. The sensitivity of the dynamic mechanical properties of water-saturated coal negatively correlated with the porosity. The dynamic weakening degree of the water-saturated coal relative to the dry coal positively relate with the porosity, which indicated that the water infusion is suitable for the coal burst prevention for the coal seam with large porosity. However, the effect of coal seam water infusion cannot be significantly exerted for the dense coal seams. In this case, the potential effective prevention method for the coal burst should select the methods, such as high intensity vibration, deep hole blasting, manual slitting, etc. to enhance the length and density of dominant fractures.

The role of porosity depends on the enhancing the scale of the dominant fractures and micro fractures to realize its effect. Specially, the former can significantly reduce the dynamic response of the coal. For the dense and high pulverized coal seams, that is, the porosity is much small, the porosity enhancement can significantly weaken the dynamic strength of coal compared with that of the coal with large porosity, as shown in Fig. 4. In this condition, the effective method to improve the effect of coal seam water infusion to prevent dynamic disaster is to increase its porosity. To achieve this, it is recommended to use the coal

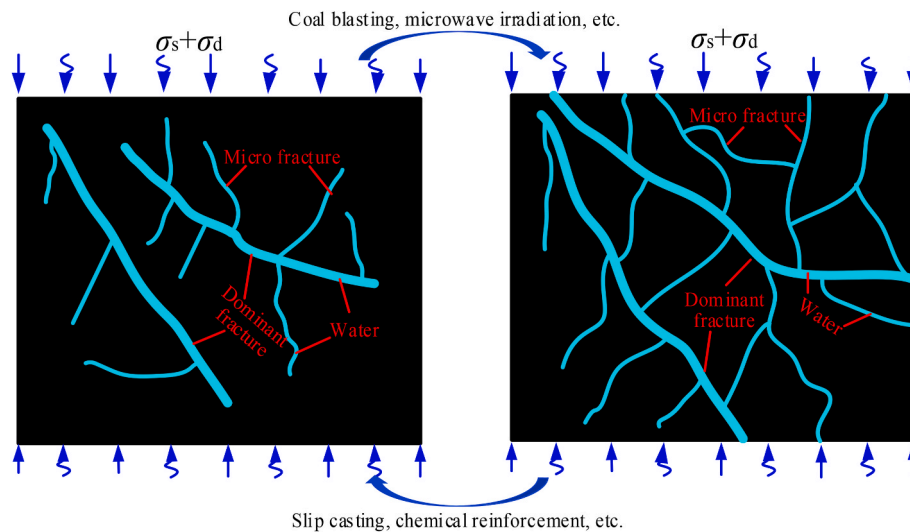


Fig. 14. Schematic diagram of coal seam treatment to prevent dynamic instability.

seam water injection coupled with other auxiliary methods, such as bottom blasting in the water infusion hole, full-drilling microwave surrounding coal breaking, etc., to increase the macro-micro damage and the porosity of surrounding coal, as shown in Fig. 14. It will enlarge the water infusion range, and fully reduce the dynamic strength of the surrounding coal, and thereby inhibiting the dynamic disaster, such as the coal burst.

However, for the water-rich coal seams with a large porosity, which not threatened by coal burst, the dynamic strength and the ability to resist the dynamic damage is weak. Subjected to the dynamic load, the coal is prone to dynamic instability, which will restricts the normal mining of the coal seam. Under this condition, the main purpose of these disasters prevention should be turned to reducing the effect of the porosity, and enhance the dynamic strength of the coal. In this case, the effective method should be to weaken the density and length of dominant fractures, reduce the number of microfractures. The alternative method is surrounding coal grouting, or adopt drainage to dry the coal seam, as shown in Fig. 14.

6. Conclusion

In this study, the water-saturated coal specimens with various porosity were prepared and tested by modified SHPB to investigate effect of porosity on dynamic mechanical properties of the water-saturated coal, and its effect mechanism. In addition, the effect mechanism of the porosity on dynamic mechanical properties of the water-saturated coal was further discussed. On this basis, the improvement methods for the dynamic stability of water-saturated coal with various porosity were further discussed. The main conclusions can be summarized as follows:

The dynamic mechanical parameters of water-saturated coal nonlinearly negatively correlate with the porosity of the specimen. The dynamic mechanical properties of water-saturated coal decrease with a gradually weakened latitude as with the increase of the porosity.

Effect mechanism of the porosity on dynamic mechanical properties of water-saturated coal around roadway was microscopically attributed to the size variation of the dominant fracture and its surrounding micro fractures. And the total cohesive force for the corresponding particles on the dominant fracture surfaces was established and applied to reveal the dominant fracture propagation mechanism.

For the dynamic disasters prevention in the coal seams with low porosity, it is recommended to enlarge the porosity before the coal seam water infusion. But for water-rich coal seams with large porosity, its dynamic stability improvement means rely on reducing the porosity by

the physical or chemical methods.

CRediT authorship contribution statement

Helong Gu: Conceptualization, Investigation, Writing – original draft. **Xingping Lai:** Methodology, Validation. **Ming Tao:** Formal analysis. **Wenzhuo Cao:** Writing – review & editing. **Zhengkai Yang:** Visualization.

Declaration of competing interest

The authors declare that they have no known competing financial interests or personal relationships that could have appeared to influence the work reported in this paper.

Data availability

The data that has been used is confidential.

Acknowledgement

The research presented in this paper was supported by the National Natural Science Foundation of China (Grant Nos.52204111).

References

- Meng Y, Li ZP, Lai FP. Experimental study on porosity and permeability of anthracite coal under different stresses. *J Pet Sci Eng.* 2015;133:810–817. <https://doi.org/10.1016/j.petrol.2015.04.012>.
- Mou PW, Pan JN, Wang K, Wei J, Yang YH, Wang XL. Influences of hydraulic fracturing on microfractures of high-rank coal under different in-situ stress conditions. *Fuel.* 2021;287, 119566. <https://doi.org/10.1016/j.fuel.2020.119566>.
- Yang T, Li B, Ye QS. Numerical simulation research on dynamical variation of permeability of coal around roadway based on gas-solid coupling model for gassy coal. *Int J Min Sci Technol.* 2018;28(6):925–932. <https://doi.org/10.1016/j.ijmst.2018.09.004>.
- Gu HL, Tao M, Cao WZ, Zhou J, Li XB. Dynamic fracture behaviour and evolution mechanism of soft coal with different porosities and water contents. *Theor Appl Fract Mech.* 2019;103, 102265. <https://doi.org/10.1016/j.tafmec.2019.102265>.
- Gu HL, Tao M, Wang JX, Jiang HB, Li QY, Wang W. Influence of water content on dynamic mechanical properties of coal. *Geotech Geol Eng.* 2018;16(1):85–95. <https://doi.org/10.12989/gae.2018.16.1.085>.
- Gu HL, Tao M, Li XB, Momeni AA, Cao WZ. The effects of water content and external incident energy on coal dynamic behaviour. *Int J Rock Mech Min Sci.* 2019;123, 104088. <https://doi.org/10.1016/j.ijrmm.2019.104088>.
- Gu HL, Tao M, Li XB, Li QY, Cao WZ, Wang F. Dynamic response and failure mechanism of fractured coal under different soaking times. *Theor Appl Fract Mech.* 2018;98:112–122. <https://doi.org/10.1016/j.tafmec.2018.09.001>.

- 8 Wang W, Wang H, Li DY, Li HM, Liu ZM. Strength and failure characteristics of natural and water-saturated coal specimens under static and dynamic loads. *Shock Vib.* 2018;2018, 3526121. <https://doi.org/10.1155/2018/3526121>.
- 9 Ai T, Wu SY, Zhang R, et al. Changes in the structure and mechanical properties of a typical coal induced by water immersion. *Int J Rock Mech Min Sci.* 2020;138, 104597. <https://doi.org/10.1016/j.ijrmms.2020.104597>.
- 10 Chen J, Cheng WM, Wang G, Li HM. Effect of dominated coal pores and fractures on water migration after low-pressure water injection based on CT images. *Fuel.* 2022; 307, 121795. <https://doi.org/10.1016/j.fuel.2021.121795>.
- 11 He MC, Miao JL, Feng JL. Rock burst process of limestone and its acoustic emission characteristics under true-triaxial unloading conditions. *Int J Rock Mech Min Sci.* 2010;47(2):286–298. <https://doi.org/10.1016/j.ijrmms.2009.09.003>.
- 12 Shang XY, Tkalčić H. Point-source inversion of small and moderate earthquakes from P-wave polarities and P/S amplitude ratios within a hierarchical Bayesian framework: implications for the Geysers earthquakes. *J Geophys Res Solid Earth.* 2020;125(2), e2019JB018492. <https://doi.org/10.1029/2019JB018492>.
- 13 Lin ZB, Zhang BY, Guo JQ. Analysis of a water-inrush disaster caused by coal seam subsidence karst collapse column under the action of multi-field coupling in Taoyuan coal mine. *Comput Model Eng Sci.* 2021;126(1):311–330. <https://doi.org/10.32604/cmescs.2021.011556>.
- 14 Li XB, Gu HL, Tao M, Peng K, Cao WZ, Li QY. Failure characteristics and meso-deterioration mechanism of pre-stressed coal subjected to different dynamic loads. *Theor Appl Fract Mech.* 2021;115, 103061. <https://doi.org/10.1016/j.tafmec.2021.103061>.
- 15 Jiang LS, Sainoki A, Mitri HS, Ma NJ, Liu HT, Zhen H. Influence of fracture-induced weakening on coal mine gateroad stability. *Int J Rock Mech Min Sci.* 2016;88: 307–317. <https://doi.org/10.1016/j.ijrmms.2016.04.017>.
- 16 Guo HJ, Yuan L, Cheng YP, Wang K, Xu C. Experimental investigation on coal pore and fracture characteristics based on fractal theory. *Powder Technol.* 2019;346: 341–349. <https://doi.org/10.1016/j.powtec.2019.02.026>.
- 17 Chan DYC, Horn RG. The drainage of thin liquid films between solid surfaces. *J Chem Phys.* 1985;83:5311–5324. <https://doi.org/10.1063/1.449693>.
- 18 De Bisschop FRE, Rigole WJL. A physical model for liquid capillary bridges between adsorptive solid spheres: the nodoid of plateau. *J Colloid Interface Sci.* 1982;88 (1982):117–128. [https://doi.org/10.1016/0021-9797\(82\)90161-8](https://doi.org/10.1016/0021-9797(82)90161-8).
- 19 Mehrotra VP, Sastry KVS. A novel method for the calculation of pendular bond characteristics between unequal-sized particles. *Powder Technol.* 1985;41:259–263. [https://doi.org/10.1016/0032-5910\(85\)80022-X](https://doi.org/10.1016/0032-5910(85)80022-X).
- 20 Wang QF, Zhao YC, Wang YL, Ai DH, Li CW. Model of stress distribution during coal roadway excavation and its numerical validation. *Arabian J Geosci.* 2020;13(4):1–11. <https://doi.org/10.1007/s12517-020-5172-8>.
- 21 Gao FQ, Stead D, Kang HP, Wu YZ. Discrete element modelling of deformation and damage of a roadway driven along an unstable goaf-a case study. *Int J Coal Geol.* 2014;127:100–110. <https://doi.org/10.1016/j.coal.2014.02.010>.
- 22 Zhou YX, Xia K, Li XB, et al. *Suggested Methods for Determining the Dynamic Strength Parameters and Mode-I Fracture Toughness of Rock Materials [M]//The ISRM Suggested Methods for Rock Characterization, Testing and Monitoring: 2007-2014.* Cham: Springer; 2012:35–44. https://doi.org/10.1007/978-3-319-07713-0_3, 2011.
- 23 Li XB, Zhou ZL, Lok TS, Hong L, Yin TB. Innovative testing technique of rock subjected to coupled static and dynamic loads. *Int J Rock Mech Min Sci.* 2008;45(2): 739–748. <https://doi.org/10.1016/j.ijrmms.2007.08.013>.
- 24 Tao M, Zhao HT, Li XB, Li X, Du K. Failure characteristics and stress distribution of pre-stressed rock specimen with circular cavity subjected to dynamic loading. *Tunn Undergr Space Technol.* 2018;81:1–15. <https://doi.org/10.1016/j.tust.2018.06.028>.
- 25 Tang SB, Yu CY, Heap MJ, Chen PZ, Ren YG. The influence of water saturation on the short-and long-term mechanical behavior of red sandstone. *Rock Mech Rock Eng.* 2018;51(9):2669–2687. <https://doi.org/10.1007/s00603-018-1492-3>.
- 26 Tao M, Ma A, Cao WZ, Li XB, Gong FQ. Dynamic response of pre-stressed rock with a circular cavity subject to transient loading. *Int J Rock Mech Min Sci.* 2017;99:1–8. <https://doi.org/10.1016/j.ijrmms.2017.09.003>.
- 27 Gu HL, Tao M, Li XB, Cao WZ, Li QY. Dynamic response and meso-deterioration mechanism of water-saturated sandstone under different porosities. *Measurement.* 2021;167, 108275. <https://doi.org/10.1016/j.measurement.2020.108275>.
- 28 Feng XT, Kong R, Zhang X, Yang C. Experimental study of failure differences in hard rock under true triaxial compression. *Rock Mech Rock Eng.* 2019;52(7):2109–2122. <https://doi.org/10.1007/s00603-018-1700-1>.
- 29 Rubin AM, Ahrens TJ. Dynamic tensile-failure-induced velocity deficits in rock. *Geophys Res Lett.* 1991;18(2):219–222. <https://doi.org/10.1029/91GL00214>.
- 30 Li XB, Gu HL, Tao M, Peng K, Cao WZ, Li QY. Failure characteristics and meso-deterioration mechanism of pre-stressed coal subjected to different dynamic loads. *Theor Appl Fract Mech.* 2021;115, 103061. <https://doi.org/10.1016/j.tafmec.2021.103061>.
- 31 Wang HL, Jin WL, Sun XY. Fracture model for protective layer cracking of reinforced concrete structure due to rebar corrosion. *J Hydraul Eng.* 2008;39(7):863–869.
- 32 Hanson JA, Hardin BO, Mahboub K. Fracture toughness of compacted cohesive soils using ring test. *J. Geotech. Eng.* 1994;120:872–891. [https://doi.org/10.1061/\(ASCE\)0733-9410\(1994\)120:5\(872\)](https://doi.org/10.1061/(ASCE)0733-9410(1994)120:5(872)).
- 33 Gu HL, Tao M, Li XB, Li QY, Cao WZ, Wang F. Dynamic response and failure mechanism of fractured coal under different soaking times. *Theor Appl Fract Mech.* 2018;98:112–122. <https://doi.org/10.1016/j.tafmec.2018.09.001>.
- 34 Zhou YX, Xia K, Li XB, Li H, Dai F. Suggested methods for determining the dynamic strength parameters and mode-I fracture toughness of rock materials. *Int. J. Rock Mech. Min.* 2011;49:105–112. <https://doi.org/10.1016/j.ijrmms.2011.10>.
- 35 Pitois O, Moucheron P, Chateau X. Liquid bridge between two moving spheres: an experimental study of viscosity effects. *J Colloid Interface Sci.* 2000;231(2000):26–31. <https://doi.org/10.1006/jcis.2000.7096>.
- 36 Lu P, Sheng ZW, Zhu GW, Fang EC. The effective stress and mechanical deformation and damage characteristics of gas-filled coal. *J China Univ Sci Technol.* 2001;31(6): 686–693.
- 37 Gu HL, Tao M, Li XB, Cao WZ, Li QY. Dynamic tests and mechanical model for water-saturated soft coal with various particle gradations. *Int J Rock Mech Min Sci.* 2020; 132, 104386. <https://doi.org/10.1016/j.ijrmms.2020.104386>.
- 38 Wang ZM, Zhou W, Jiskani IM, et al. Dust reduction method based on water infusion blasting in open-pit mines: a step toward green mining. *Energy Sources Part A.* 2021: 1–5 <https://doi.org/10.1080/15567036.2021.1903118>.
- 39 Freund LB. *Dynamic Fracture mechanics[M].* Cambridge university press; 1998.